Sensors & Actuators: A. Physical 374 (2024) 115466

Contents lists available at ScienceDirect

Sensors and Actuators: A. Physical

journal homepage: www.journals.elsevier.com/sensors-and-actuators-a-physical

Narrow-band n-GaN/n-Si isotype heterojunction photodiode: A simplified approach for photodiode development

Ali Olkun [a], Hüseyin Kaan Kaplan [a], Sertan Kemal Akay [a,*], Muhitdin Ahmetoğlu [a], Suat Pat [b], Nursev Erdoğan [c]

[a] Department of Physics, Faculty of Arts and Science, Bursa Uludağ University, Nilüfer, Bursa 16059, Turkey
[b] Department of Physics, Faculty of Science, Eskişehir Osmangazi University, Meşelik, Eskişehir, Tukey
[c] TUSAŞ Aerospace Industries Inc, Ankara, Turkey

ARTICLE INFO

Keywords:
Narrow-band self-powered photodiodes
N-n isotype heterojunction
GaN thin film growth
Near-infrared
Photoresponsivity

ABSTRACT

An innovative approach has been explored to fabricate a high-performance photodiode in semiconductor device production, utilizing the thermal evaporation technique to grow GaN thin films. Structural analyzes were conducted on both as-deposited and annealed samples, and their properties were determined using various characterization techniques, including FESEM, XRD, XPS, Hall effect, photoluminescence, and UV-Vis spectrophotometer measurements. Valuable information has been gained about the potential of this alternative approach for fabricating GaN-based electronic devices. In this study, Al/n^+-GaN/n-Si/Ag (as-deposited GaN) and Al/n-GaN/n-Si/Ag (annealed GaN) structures have been fabricated. It was found that the device produced from the as-deposited GaN thin film exhibited better performance than the annealed one. The isotype heterojunction n^+-GaN/n-Si photodiode exhibited exceptional performance in detecting NIR light at a wavelength of 1050 nm under a 0 V bias. It has a full-width at half-maximum (FWHM) value of 120 nm and achieved a photoresponsivity value of 355 mA/W at a light output of 10 mW/cm^2. It is further supported by its external quantum efficiency of 42% and detectivity value of 6.93×10^{11} Jones at the peak wavelength and very fast response speed with ~33 μs rise/fall times. These findings highlight the potential of photodiode as an efficient narrow-band in the NIR region.

1. Introduction

III-N semiconductor structures (GaN, InN, AlN) and their ternary compounds are commonly used in semiconductor device fabrication due to their direct and wide band gaps (0.7–6.2 eV). Photodiodes (PDs), high-power transistors, light-emitting diodes (LEDs), laser diodes (LDs), and high electron mobility transistors (HEMTs) can be given as examples of such devices. These electronic components have applications in various areas, such as the automotive industry, military applications, aerospace, and many other fields [1–12]. PDs are produced using Schottky, metal-semiconductor-metal (MSM), metal-oxide-semi conductor (MOS) structures, and other semiconductor junctions [13–15]. Besides, they are categorized into two groups based on the width of their responsivity spectrum: broadband and narrow-band PDs [16–18]. Broadband PDs are commonly used due to the wide absorption ranges of semiconductor materials. Although broadband PDs have a wide application area, some applications require narrow-band PDs that can operate in specific wavelength ranges. It can provide a narrow-band detection feature by adding optical filters to broadband PDs. However, achieving narrow-band detection capability through optical filters brings disadvantages such as larger device sizes, design complexity, and higher prices. For this reason, producing cost-effective, filterless narrow-band PDs with desired sizes has become crucial. In recent studies, organic semiconductors and perovskite materials have been preferred for fabricating narrow-band photodiodes since they exhibit true-narrow-band absorption behavior. They also have disadvantages such as potential instability, limited operational lifespan, and cost implications [19,20]. Plasmonic grating-enhanced Schottky narrow-band PDs are available; however, their production requires techniques such as e-beam deposition and lithography [21]. Hyper-doped Si-based narrow-band PDs produced using femtosecond laser melting and surface doping with chalcogens (S, Se, Te) and transition metals (Au, Ti, Ni). Still, their manufacturing processes are costly [22]. The narrow-band n^+-GaN/n-Si heterojunction PDs produced in this study are based on a

* Corresponding author.
E-mail address: kakay@uludag.edu.tr (S.K. Akay).

https://doi.org/10.1016/j.sna.2024.115466
Received 4 January 2024; Received in revised form 30 April 2024; Accepted 11 May 2024
Available online 14 May 2024
0924-4247/© 2024 Elsevier B.V. All rights are reserved, including those for text and data mining, AI training, and similar technologies.

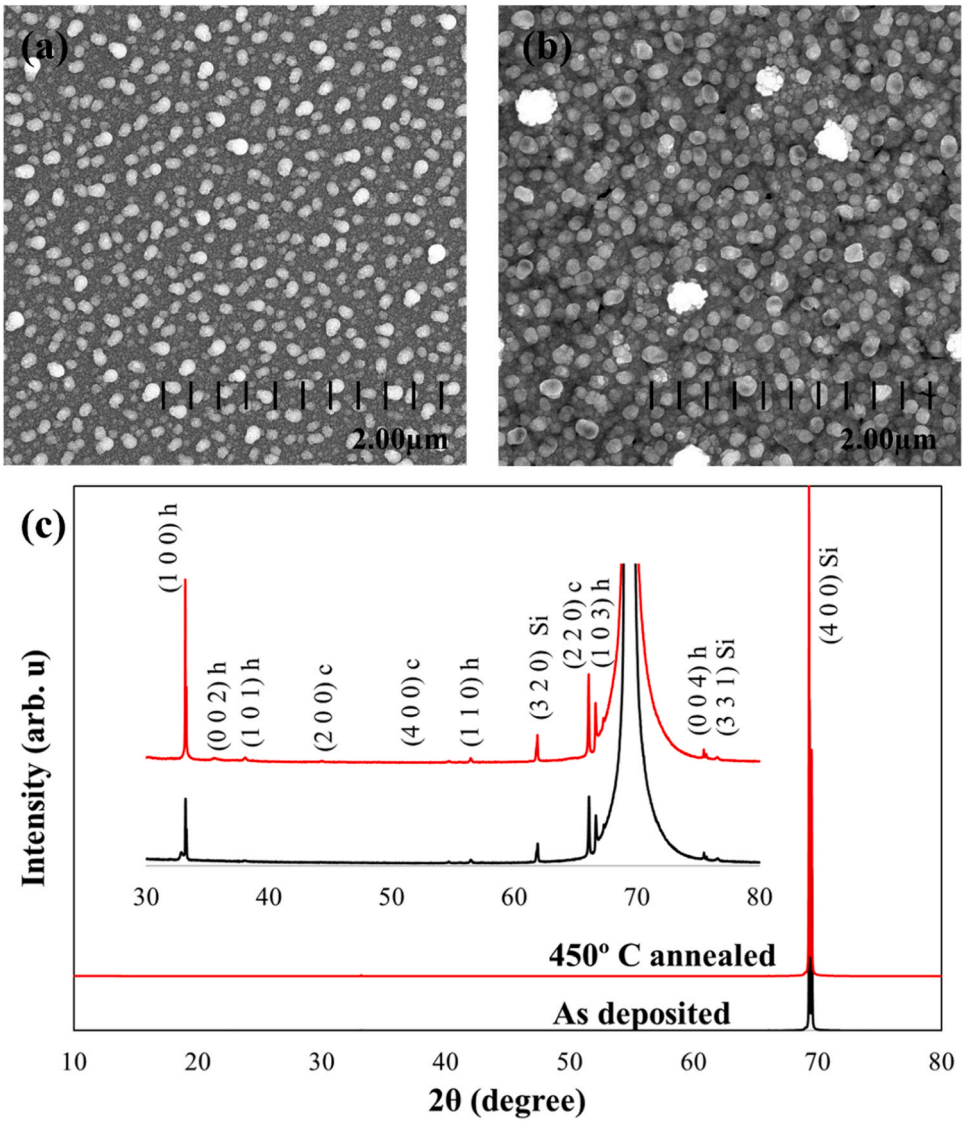


Fig. 1. FESEM images of the GaN layer deposited on n-Si substrate, both in the (a) as-deposited condition and (b) after annealing at 450°C, (c) XRD patterns.

charge-collection-narrowing (CCN) process similar to that in hyper-doped Si PDs. Besides, its production technique is simpler and more economical.

In the growth of GaN thin films, methods such as metal-organic chemical vapor deposition (MOCVD), metal-organic vapor phase epitaxy (MOVPE), and molecular beam epitaxy (MBE) are commonly employed [23–25]. Until now, various III-N-based photodiode structures have been fabricated and investigated. Some of these studies are outlined below. A MoS_2/GaN p-n photodiode has been reported to exhibit self-driven operation in the 265 nm deep ultraviolet (DUV) range and has a photoresponsivity of 187 mA/W [26]. A p-GaN/n-ZnMgO structure demonstrated a zero-bias response of 196 mA/W under 362 nm UV illumination, with turn-on and turn-off times of 1.7 ms and 3.3 ms, respectively [27]. Neha Aggarwal et al. investigated the charge transport mechanisms of different metals (Au, Ti/Al, and Al) in GaN-based metal semiconductor metal MSM structures [6]. Beyond p-n junctions, n-n and p-p isotype structures exhibit distinct characteristics, most notably wavelength-dependent polarity-switching behavior [28,29]. Variable polarity enables photodiodes to operate at different wavelengths depending on the applied voltage. Furthermore, isotype structures with self-driven capabilities are also present in narrow-band photodiode applications. For instance, Georgios Chatzigiannakis and his team developed a wide spectral range variable-polarity n^+-ZnO/n-Si heterojunction photodiode. They demonstrated its operation under various bias conditions in the UV–visible and near-infrared (NIR) regions [16]. In addition to these studies, self-driving wavelength-selective p-SnS/p-Si heterojunction devices are available [17]. Recently, a study reported the production of self-driven, filterless, narrow-band p^+Cu_2S/p-Si isotype heterojunction structures operating in the near-infrared region, which resulted in improved performance outcomes [30].

In this study, a thermal evaporation (TE) device was employed for GaN thin film growth, followed by annealing of the films in a Nitrogen (N_2) environment at 450°C for 30 minutes. The electrical and structural properties of the as-deposited and annealed structures were examined using FESEM, XRD, XPS, Hall Effect measurements, PL, and a UV-Vis spectrophotometer. According to the literature review, no published article exists in which thermal evaporation is used as a different method for conventional epitaxial GaN thin film growth, apart from the conventional method. The advantage of this method in this study over epitaxial thin film growth methods includes a rapid production process, environmentally friendly, absence of toxic gas emissions, no requirement for precursor solutions during production, and no need for extra filtration within the vacuum system. The electrical and structural

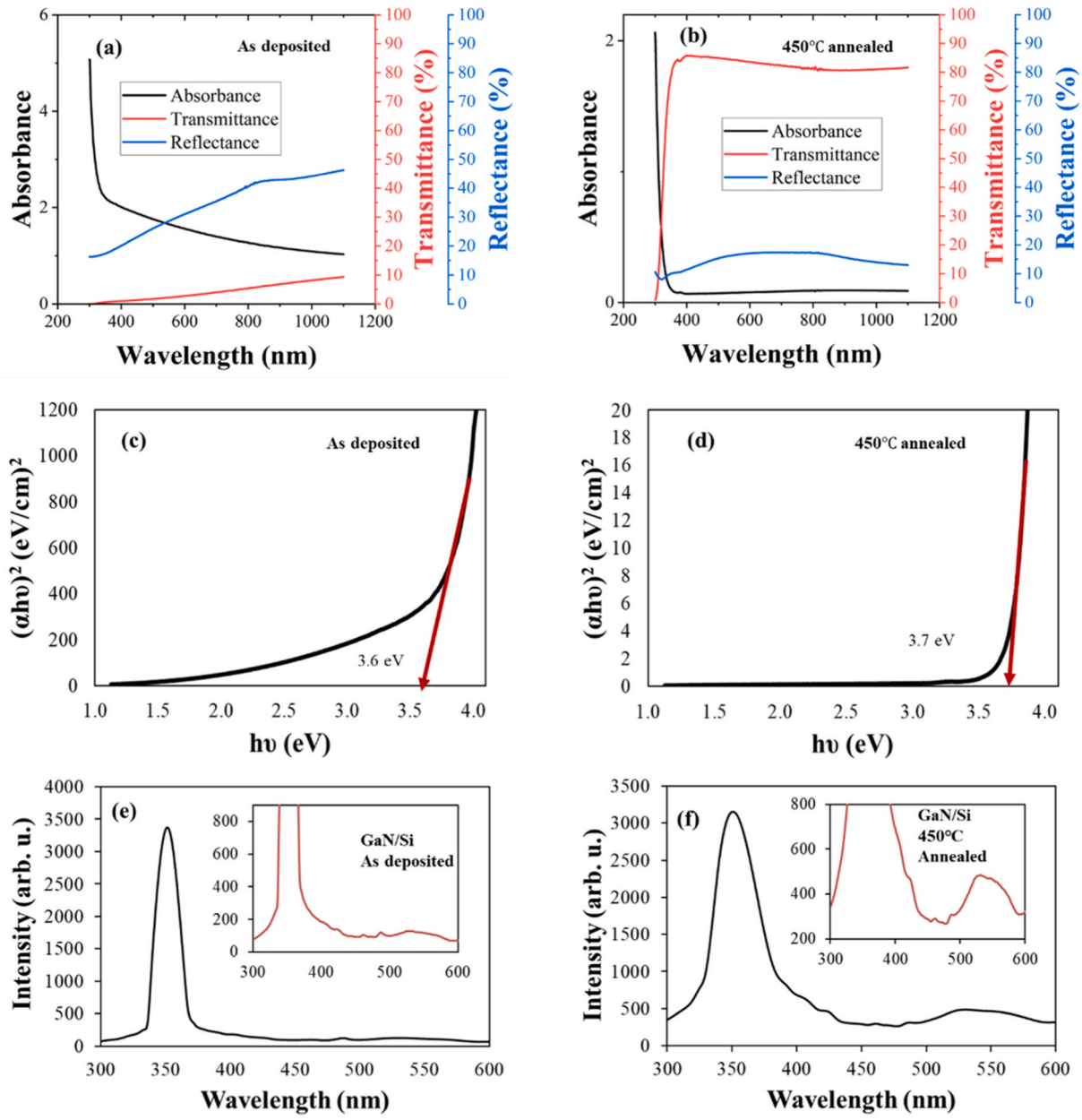


Fig. 2. Absorption, transmittance, and reflectance graphs corresponding to wavelength are shown for (a) as-deposited, (b) annealed at 450°C, as well as the Tauc plot for (c) as-deposited and (d) annealed samples. Photoluminescence spectra of the GaN thin film grown on (100) n-Si substrate, showing (e) as-deposited (n^+-GaN/n-Si) and (f) 450°C annealed (n-GaN/n-Si).

properties of as-deposited and annealed samples were determined, followed by the analysis of the photodiode properties of the n-GaN/n-Si isotype heterojunction structure. The results show that the photodiode properties of the Al/n^+-GaN/nSi/Ag heterojunction outperformed those of the annealed structure. The Al/n^+-GaN/nSi/Ag heterojunction demonstrated a narrow-band photodiode with a full-width at half-maximum (FWHM) of 120 nm at wavelength of 1050 nm and a photoresponsivity of 355 mA/W under zero-bias conditions. This study presents the successful development of a cost-efficient GaN-based photodiode with narrow-band detection capability achieved through a straightforward fabrication process.

2. Experimental section

The GaN thin films were produced using the physical vapor deposition method known as TE. In this method, the desired material is evaporated by heating it to high temperatures under a high vacuum and deposited on the desired material. In comparison to traditional epitaxial thin film growth methods, the TE method employed in this study offers several advantages. Among these advantages, since there is only nitrogen gas and GaN pellet in the chamber during coating, nitrogen gas is released into the atmosphere during production. In this case, there is no harm to the environment, and there is no need for additional filtration in the vacuum system. There is no need for precursor chemicals to be added when evaporating GaN pellets.

Cleaning of the glass and Si substrates involved a 10-minute treatment with deionized water, acetone, and isopropanol, respectively. Then, they were dried using a high-purity dry nitrogen gas blow. To eliminate the native oxide layer on the Si substrates, a chemical etching process was performed for 1 minute in a 10% (v/v) HF acid solution. This was followed by rinsing with deionized water and drying with nitrogen gas. The GaN powder material with a purity of 99.99% (Alfa

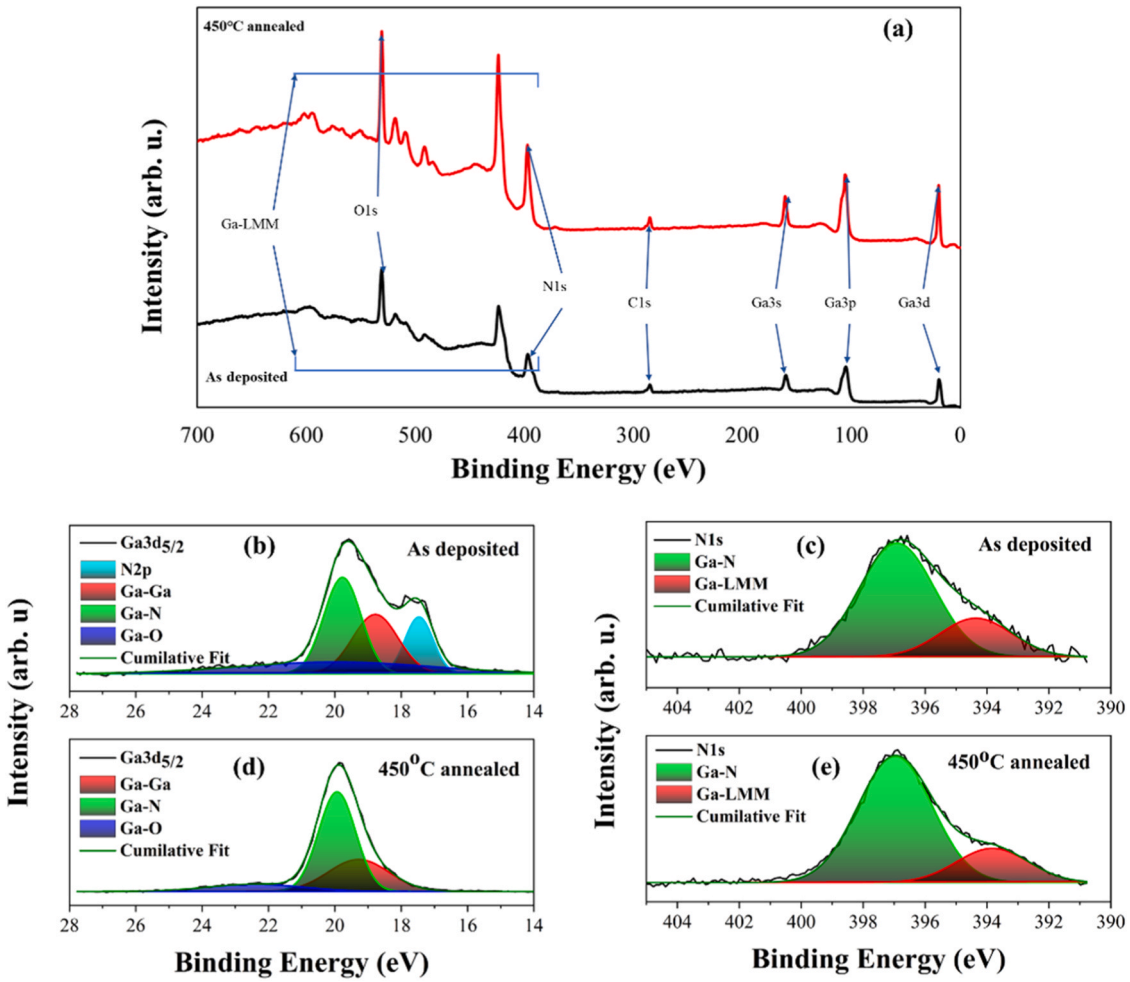


Fig. 3. Surface analysis of the GaN thin film deposited on n-Si using X-ray Photoelectron Spectroscopy (XPS) (a), Ga 3d core level and N1s core level (b and c) as-deposited, (d and e) annealed at 450°C, respectively.

Aesar) was pelletized and placed within the TE source. Then, soda lime glass and n-Si substrates, each measuring 25×25 mm^2, were positioned 16 cm above the evaporation source, and the vacuum chamber was sealed. The chamber was vacuumed until reaching a base pressure of 5×10^{-6} torr through mechanical and turbomolecular pumps. Subsequently, nitrogen gas was introduced through a mass-flow controller, and the evaporation was conducted at a 2×10^{-4} torr partial pressure of N_2 with an evaporation source current of 186 A. The thickness of the GaN thin film was measured as 50 nm during the deposition with two Quartz Crystal Microbalances (QCM).

GaN thin films were annealed under nitrogen flow at 450°C for 30 min. To evaluate the diode properties of GaN thin films, n^+-GaN/n-Si (as-deposited) n-GaN/n-Si (450°C annealed) heterojunction structures were fabricated. Ohmic contacts (Fig. S3, Supporting Information) on the n-GaN side involved the deposition of 100 nm-thick aluminum (Al) contacts in the shape of point contacts with a diameter of 1.5 mm. This process was carried out using a dot-shaped shadow mask. For n-Si, 100 nm thick silver (Ag) metal was chosen as the back ohmic contact. These contact metals were chosen to achieve better ohmic behaviors for Si wafer and GaN thin film layers. While an ohmic contact occurs between Al metal and n-GaN, a Schottky barrier forms between Al and n-Si, thus Ag metal was used to obtain ohmic contact on n-Si [31–33].

The structural and electrical properties of as-deposited and annealed GaN thin films were investigated. For electrical characterization, a Ecopia HMS 3000 Hall Effect measurement system was utilized. Optical transmittance, absorbance, and reflectance measurements of samples coated on glass were determined using the Shimadzu UV-2600 UV-Vis Spectrophotometer. Photoluminescence measurements were conducted on the GaN/Si structures using the Perkin-Elmer LS-55 tool. The surface morphology of the thin films was imaged using a scanning electron microscope (Hitachi Regulus 8230 FE-SEM). The crystal structure was determined using the Panalytical EMPYREAN X-ray Diffraction (XRD) apparatus. Thermo-Scientific K-Alpha X-ray Photoelectron Spectrometer (XPS) was used to identify molecular structure. The energy of the X-ray source used was 1486.7 eV Al-Kα, and data were acquired from a depth of 10 nm below the surface.

3. Results and discussion

The surface FESEM images of n-Si substrates (100) with grown GaN thin films are shown in Fig. 1a and b. Upon examination, the images reveal the homogeneous distribution of GaN over the surface. The FESEM image presented in Fig. 1a corresponds to the GaN sample as it was deposited. The small, bright, and spherical shapes observed in the image indicate regions, where Gallium (Ga) atoms are densely accumulated, with the intensity, spread uniformly across the entire surface. In Fig. 1b, the image belongs to a sample that was annealed in a nitrogen environment at 450°C for 30 minutes. It can be seen in Fig. 1b that the density of bright spherical structures dispersed over the surface, associated with metallic Ga decreases with annealing.

The crystalline properties of GaN thin films deposited on (100) Si wafers using the TE method were investigated through X-ray diffraction (XRD). The as-deposited and annealed (450°C) GaN thin films were analyzed. The obtained diffraction pattern was compared to literature

2theta values, and peaks were matched, as shown in Fig. 1**c** (PDF Entry No. 01–070–2562, 01–076–0703, 01–079–0622, and 01–079–2499). The XRD analysis revealed that the (100) oriented dominant hexagonal phase at 33.18° becomes more prominent after annealing.

Optical measurement results of the as-deposited and 450°C annealed samples are presented in Fig. 2a and b. Fig. 2a displays the absorption, transmission, and reflection results against wavelength for the as-deposited sample. FESEM/EDS (Fig. S1, Supporting Information) and XPS analyses show that GaN loses nitrogen and becomes enriched in Ga during evaporation.

Consequently, the sample exhibits low transmittance and high reflection due to its metallic surface. Fig. 2b provides the results for the samples after annealing. The annealing process facilitates the N-bonding of N-deficient GaN and metallic Ga in the material, leading to the expected increase in optical transmittance.

Utilizing the optical data, the $(\alpha h\nu)^2$–$h\nu$ graphs obtained through the Tauc equation are presented in Fig. 2c and d [34]. The points where the tangent lines drawn from the linear segments of these graphs intersect the $h\nu$ axis correspond to the energy band gap (Eg) values of the thin films. For the as-deposited and 450℃ annealed samples, the Eg values were determined to be 3.6 eV and 3.7 eV, respectively. In literature, GaN produced using single crystal growth methods typically exhibits a band gap of around 3.4 eV [35]. The higher Eg value observed in this study can be attributed to the interaction of oxygen atoms with Ga in the molecular structure, which is a result of the deposition method [36].

The photoluminescence measurements of the as-deposited and 450°C annealed GaN thin films are depicted in Fig. 2e and f. In Fig. 2e, the dominant ultraviolet (UV) peak in the as-deposited thin film was attributed to the recombination of electron-hole pairs in GaN. However, inset graphs show the visible photon emissions within the material and at the heterojunction interface. [37–40].

This photon emission is due to the broad deep-level (DL)-associated emission (or trap-state emission) in the visible range attributed to the surface and interface defects in the heterojunction. The ratio of UV (300−425) and DL (425−600) emission peaks (I_{UV}/I_{DL}) obtained from PL measurements is the ratio that allows us to understand the surface defects in the material. Here, a low I_{UV}/I_{DL} ratio corresponds to high-density surface defects, while a high I_{UV}/I_{DL} ratio corresponds to low-density surface defects [41–43]. The I_{UV}/I_{DL} ratios obtained for the as-deposited and 450°C annealed materials were calculated as 4.942 and 2.589, respectively.

Under normal conditions, annealing is expected to reduce defect-related interband emissions [16]. However, it was observed that the photoluminescence intensity in the visible range increases, as depicted in the inset graphs, contrary to the expected reduction due to defect-related emissions (see Fig. 2e and f).

When the as-deposited material is excited, it is hypothesized that photon emissions from defect states are recaptured by photon traps within the material, making them undetectable by the detector. On the other hand, in the 450°C annealed thin film, the reduction in defect density and the decrease in trap-related emissions in intermediate states allow defect-related photon emissions to be detected by the detector without being trapped within the material. Hence, it may be thought that the intensity value of the annealed material increases due to these factors.

XPS was utilized to provide detailed insights into the molecular structure of the fabricated thin films by providing information about the elemental-level electronic states of the material. Fig. 3**a** illustrates the general surface scan graph obtained from the XPS analysis of the GaN thin film, with identified peaks corresponding to Ga3d, Ga3p, Ga3s, C1s, N1s, Ga-LMM, and O1s. Furthermore, the peaks identified in this study correlate with those found in the literature [44–53].

In the XPS spectrum of the Ga3d region shown in Fig. 3b, when the as-deposited sample was deconvoluted, it was determined that four distinct sub-peaks emerged. The main component of the Ga3d peak corresponds to the Ga-N peak with a binding energy of 19.77 eV[47,50,54]. The sub-peak with a binding energy of 18.78 eV corresponds to Ga-Ga bonding[47,54]. The sub-peak at 17.46 eV arises from overlapping N2s states [47,55]. The sub-peak with a binding energy of 20.00 eV represents the Ga-O bond [44,47,54]. In Fig. 3d, upon examining the XPS graph of the thin film annealed at 450℃, it can be observed that the N2s state has disappeared. The absence of the N2s state and the decrease in the intensity of the Ga-Ga peak indicate a strengthening of the Ga-N bond. Besides, the shift of the Ga-N peak from 19.77 eV to 19.95 eV shows that O atoms are also bonded into the Ga-N structure. The likely reason for the increase (3.6 eV to 3.7 eV) in bandgap is probably due to the formation of Ga-O bonds. The Ga-O bond has greater ionicity than Ga-N, as O (3.5) electronegativity is greater than that of N (3.0), leading to an increase in the bandgap[56–60].

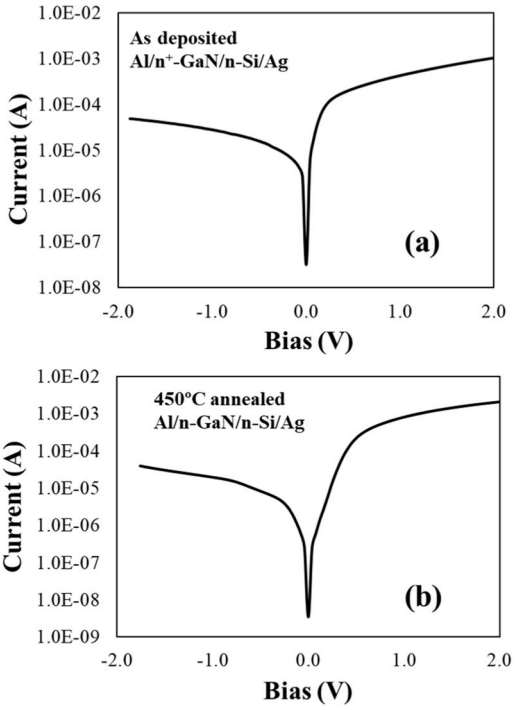


Fig. 4. Semi-logarithmic current-voltage (I-V) curves of the n-n isotype heterojunction, grown on (100) n-Si substrate, in (a) as-deposited (Al/n^+-GaN/n-Si/Ag), and (b) 450°C annealed (Al/n-GaN/n-Si/Ag).

The N1s graphs in Fig. 3c and **e** show different bonding states of nitrogen. Upon examining the XPS data of GaN films in the literature, it is observed that the energy of the N1s peak is generally close to the characteristic binding energy of the Ga-N bond, which is typically around 396.9 eV [37,45,50,61]. However, variation in chemical states or surface interactions can lead to shifts in the binding energy of the N1s peak. When nitrogen atoms bond with oxygen or interact with other elements, the binding energy of the N1s peak can change [37]. In Fig. 3c, the satellite peak at a binding energy of 394.3 eV next to the N1s peak indicates the Ga-LMM peak. In the graph presented in Fig. 3e, it can be observed that this satellite peak has shifted to an energy level of 393.8 eV [45]. This peak represents different bonding states of Ga. The letter "L" indicates that photoelectrons originate from the inner shells of Ga (L shell). "MM" denotes the energy levels of photoelectrons from the outer shells (M shell) of Ga. The presence of Ga-LMM peaks indicates the existence of various chemical states of Ga and suggests different bonding environments. For instance, Ga atoms might have different oxidation states or might have interacted with other elements on the surface.

The current-voltage measurements were conducted for the Al/n^+-GaN/n-Si/Ag and Al/n-GaN/n-Si/Ag heterojunction diodes to determine their diode parameters. The measurements were conducted within the ±2 V bias range, and semi-logarithmic current-voltage curves were plotted, as depicted in Fig. 4a and b.

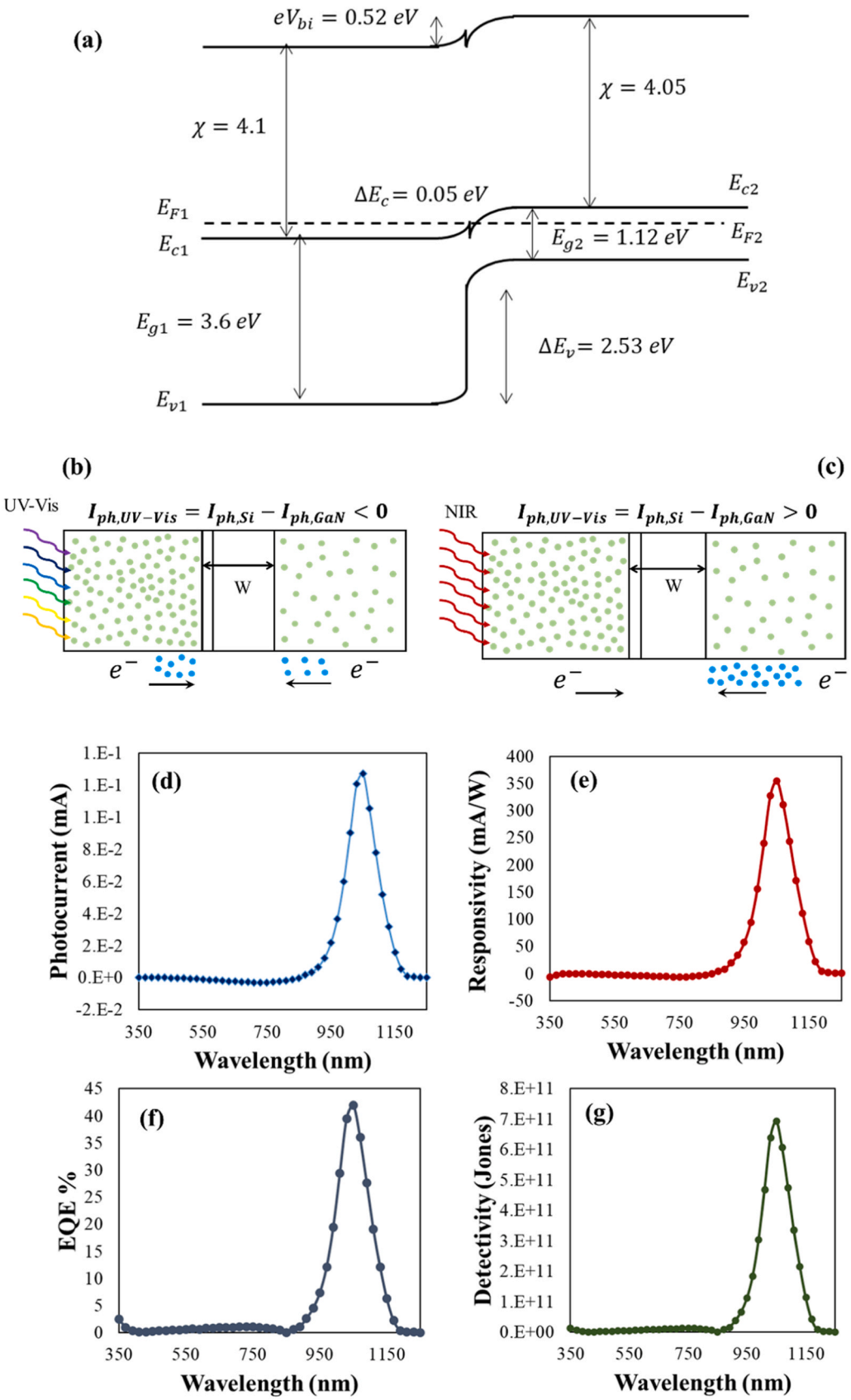


Fig. 5. As deposited n^+-GaN/n-Si photodiode under zero bias, (a) Energy band diagram, (b) Illumination in the UV-Vis region, (c) Illumination in the infrared region, (d) Photocurrent, (e) Photoresponsivity, (f) External Quantum Efficiency (EQE), and (g) Detectivity (D).

Table 1
Comparison of n^+-GaN/n-Si and n-GaN/n-Si self-powered narrow-band near-infrared photodiodes with leading narrow-band NIR photodiodes in the literature.

Device	Bias (V)	λ (nm)	R_λ (mA/W)	D* (Jones)	EQE (%)	FWHM (nm)	Rise/Fall Times (μs)	References
Al/n^+-GaN/n-Si/Ag	**0**	**1050**	**355**	**6.93×10^{11}**	**42**	**120**	**33.8 / 33.0**	**This work**
Al/n-GaN/n-Si/Ag	**0**	**1090**	**9**	**5.40×10^{10}**	**1**		**34.8 / 78.7**	**This work**
CuGaTe2/Si	0	1050	114	2.01×10^{12}	71 (-3 V)	~118		[18]
MAPb(I_yBr_{1-y})$_3$/ glass/ITO/PEDOT:PSS/ MAPb(I_xBr_{1-x})$_3$/PCBM/Ag	0	1100	331	4.27×10^{10}	50	~50	~180 / 200	[19]
ITO/PEDOT:PSS/DPP-DTT:PCTOBM/C_{60}/Al	1	950	52	10^{12}	8	<90	-	[20]
ITO/PEDOT:PSS/ P3HT:BEH:F6TCNNQ /Al	-13	850	27		29,700		624×10^3	[21]
Si:Ag	-3	1310	504		48		~179	[22]
InGaN/Si	0	1060	0.25			120		[64]
ITO/SnO_2/PDTP-DFBT:PC71:BM:PbS-QDs/BCP/Ag	-7	890	1310	7.98×10^{11}	183	<50	14.8 / 32	[65]
Perovskite/glass/ITO/CuPc/C_{60}:PbPc/C_{60}/BCP/Al	-5	808	1090	2.23×10^{11}	167	~60		[66]

When the carrier concentrations of the grown GaN thin films were measured using the Hall Effect, the as-deposited sample exhibited a carrier concentration of 6.17×10^{22} cm^{-3}. In contrast, the sample annealed at 450°C showed a reduced value of 2.3×10^{12} cm^{-3}. Additionally, the carrier concentration of the n-Si substrate was determined as 4.97×10^{14} cm^{-3} via Hall Effect measurement.

The difference in carrier concentrations between the heterojunction indicates the presence of a one-sided band bending, which implies that the current-voltage characteristics adhere to the Theory of Thermionic Emission [62]. For both the Al/n^+-GaN/n-Si/Ag and Al/n-GaN/n-Si/Ag heterojunction diodes, the ideality factor, saturation current, and barrier height values were calculated using the thermionic emission theory. For the as-deposited sample, these values were 1.98, 6×10^{-6} A, and 0.65 eV, while the values for the annealed sample were 2.03, 3×10^{-6} A, and 0.66 eV, respectively. **(**Eq. S1, S2, S3, S4 Supporting Information**)**

One of the essential characteristics of a photodiode is its photoresponsivity. Photoresponsivity is related to how much current the photodiode generates in response to the intensity of incident light on the surface. For both the n^+-GaN/n-Si and n-GaN/n-Si isotype heterojunction structures, under zero-bias conditions, spectral light responsivity measurements were conducted based on the photon wavelength. The responsivity spectra presented in Fig. 5e and 6e were calculated using the photocurrent spectra shown in Fig. 5d and 6d and the expression for R_λ given by Eq. (1). [30]

$$R_\lambda = \frac{I_{ph}}{P_\lambda} = \frac{I_\lambda - I_d}{E_\lambda \bullet S} \quad (1)$$

Here, I_{ph} photocurrent, P_λ is the incoming light power, I_λ is the photocurrent, I_d is the dark current, E_λ is the light power density **(**Fig. S2**,** Supporting Information**)**, and S is the effective illuminated area. For the n^+-GaN/n-Si photodiode, the measured photocurrent value at the peak wavelength around 1050 nm is 0.13 mA under zero-bias conditions, and the photoresponsivity value is calculated to be 355 mA/W. The External Quantum Efficiency (EQE) and Detectivity (D) values (Eq. S5, S6, Supporting Information) at the same peak wavelength are calculated as 42% and 6.93×10^{11} Jones, respectively (Fig. 5f and g) [30] which are a good compared to literature (see Table 1).

In Fig. 5d and e, the photocurrent and spectral photoresponsivity values of the as-deposited material exhibit negative currents within the range of 350 nm to 870 nm. This switching polarity between negative and positive currents is observed in isotype heterojunction structures [16,17,28–30]. The phenomenon of switching polarity can be explained via the energy band diagram. Electrons in both sides' conduction bands of the photodiode can easily cross the ΔEc value, contributing to the diffusion current [62,63]. However, holes in the valence band can only pass across from the n^+-GaN side to the n-Si side due to the high ΔEv value [62,63]. The energy band diagram of the n+-GaN/n-Si photodiode is provided in Fig. 5**a**. According to this diagram, when the photodiode is illuminated in the UV-Vis range (350 – 870 nm), it can be observed that the electron in electron-hole pairs generated on over-doped n^+-GaN side easily surpass the ΔEc threshold and migrate to the n-Si side, thereby contributing to the diffusion current. To gain a more detailed understanding of this mechanism, photoluminescence (PL) measurement was utilized. In GaN produced using single crystal growth methods, defects are minimal. Consequently, photons are not absorbed when exposed to visible and longer wavelengths; thus, no photocurrent is generated. However, the GaN thin films produced in this study were not single crystals and did not exhibit a higher defect density. The peak in the UV region of the PL graph arises from the recombination of electron-hole pairs in GaN. In contrast, the peaks in the visible region stem from intermediate band levels caused by defects within the material. As a result, a portion of the visible light spectrum is captured by photon traps within the GaN before reaching the n-Si side. Consequently, the contribution of the photocurrent generated on the n-Si side decreases. Since the photocurrent generated on the n^+-GaN side is greater than that generated on the n-Si side, a negative polarity current is formed [16,17, 28–30]. Therefore, as in the current transport mechanism shown in Fig. 5b, in the photodiode illuminated in the UV-Vis region (350 – 870 nm), the resulting net photocurrent was shifted to the negative region. In Fig. 5c, when the photodiode was illuminated in the NIR region (870–1250 nm), the photons passed through the n^+-GaN region and were absorbed by the n-Si side, forming electron-hole pairs**.** From these formed electron-hole pairs, electrons can easily pass to the other side, but holes cannot surpass the high ΔEv value and begun to accumulate. Therefore, the photocurrent was only generated on the n-Si side, producing a positive photocurrent [16]. Comparison of n^+-GaN/n-Si and n-GaN/n-Si self-powered narrow-band near-infrared photodiodes with the leading narrow-band NIR photodiodes in the literature are given in Table 1**.**

The photoresponsivity graph presented in Fig. 6e for the photodiode annealed at 450°C was explained using the energy band diagram and photoluminescence measurements. The energy band diagram of the n-GaN/n-Si photodiode is shown in Fig. 6a. According to the Hall Effect measurement, the annealing process reduced the carrier concentration of GaN to a value of 2.3×10^{12} cm^{-3}. When examining the band diagram of the photodiode, it is observed that the ΔEc value in the conduction band is tiny. In this case, it is considered that the energy of the incoming photons on the photodiode will be sufficient to overcome the ΔEc value of electrons and contribute to the photocurrent.

When the photodiode is illuminated in the UV-Vis region, it can be seen from the absorption spectrum (see Fig. 2b) that photons with wavelengths shorter than 350 nm are absorbed by GaN. Therefore, most photons with wavelengths longer than 350 nm pass to the n-Si side, where they are absorbed to generate electron-hole pairs. Still, it can be seen in Fig. 2f that some of the photons are captured by the trap levels. As a result, electrons from the electron-hole pairs formed on the n-Si side overcome the small ΔEc and pass to the n-GaN side, creating a positive photocurrent (see Fig. 6b).

When light was directed to the photodiode in the NIR spectrum, a situation similar to that in the as-deposited photodiode emerged (Fig. 6c). Photons reached the n-Si side of the photodiode, resulting in the formation of electron-hole pairs. Electrons moved across the

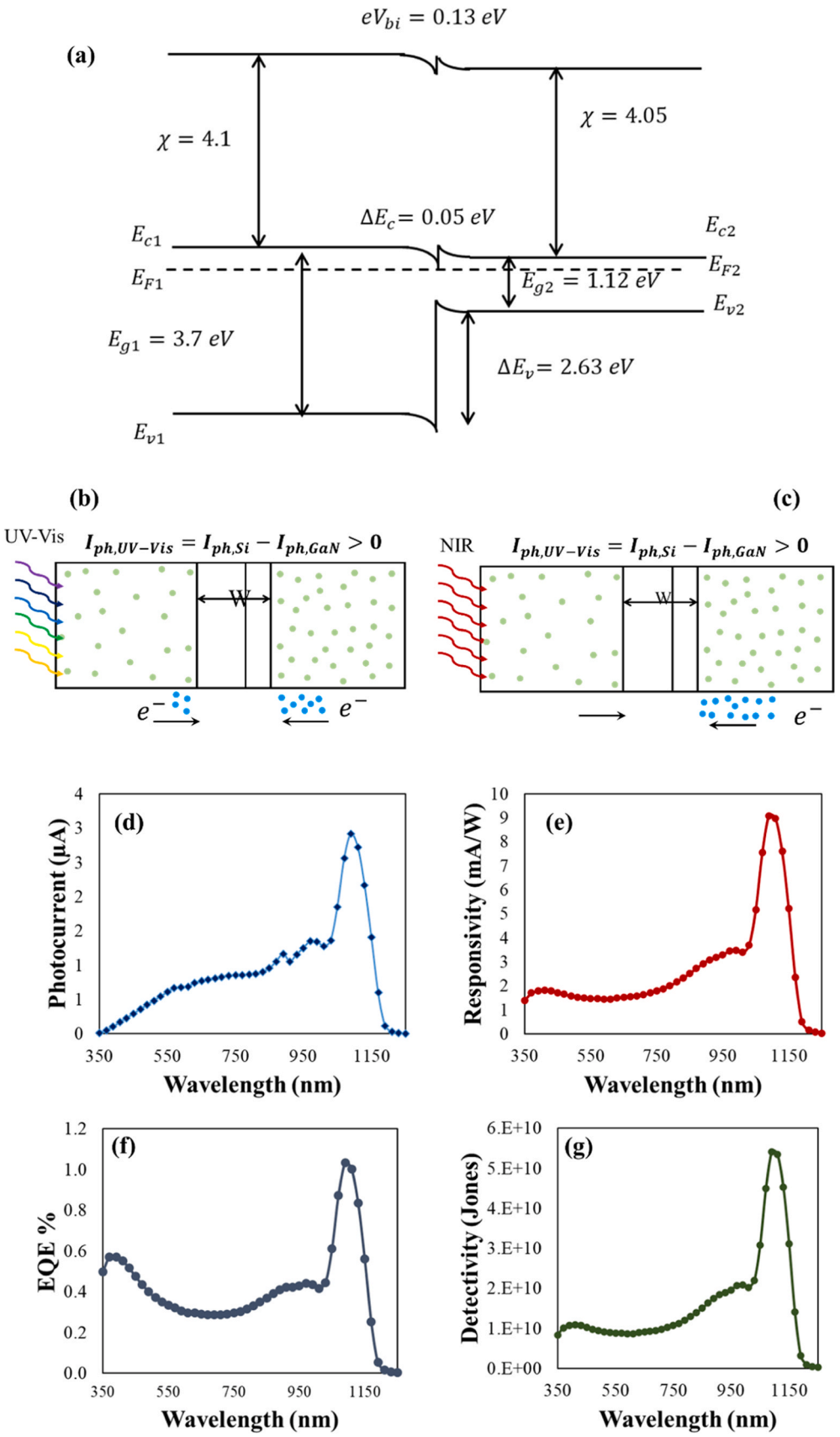


Fig. 6. 450°C annealed n-GaN/n-Si photodiode under zero bias, (a) Energy band diagram, (b) Illumination in the UV-Vis region, (c) Illumination in the infrared region, (d) Photocurrent, (e) Photoresponsivity, (f) External Quantum Efficiency (EQE), and (g) Detectivity (D).

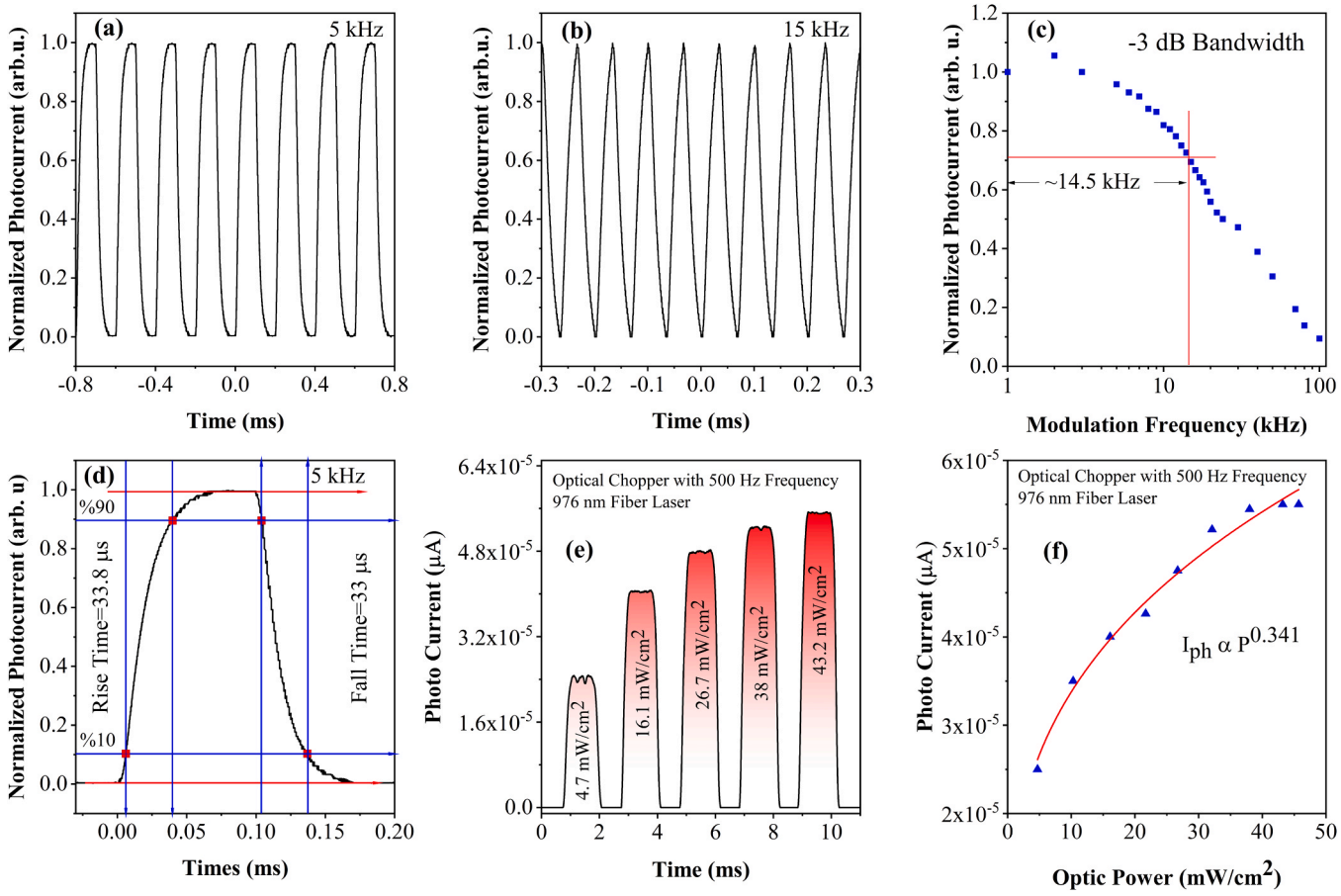


Fig. 7. Transient photocurrent was investigated during the illumination of an Al/n+-GaN/n-Si/Ag photodiode, employing a 940 nm infrared light-emitting diode (LED) modulated by a function generator for (a) 5 kHz and (b) ~15 kHz cut off frequency (c) modulation frequency dependence of normalized photocurrent and 3 dB bandwidth of the device at zero bias. (d) Normalized photocurrent in one cycle to show the rise and fall time. (e) Photocurrent with 976 nm fiber laser at different powers at the optical chopper with 500 Hz frequency (f) Photocurrent as a function of the power of incident light for 976 nm fiber laser.

conduction band to the GaN side to generate a photocurrent, while the holes could not overcome the high ΔEv value and started accumulating. As seen in the photoluminescence spectrum (Fig. 2f), interband states corresponding to shorter wavelengths trap some of these photons. Thus, it prevents some of the photons from passing through and being absorbed by the n-Si side, causing the photocurrent to decrease at wavelengths below 870 nm. The photocurrent shows a sudden increase in the wavelength range between 870 nm and the absorption edge of Si. Under zero bias voltage, a maximum photocurrent value of 2.9 µA was measured at a wavelength of 1090 nm in this context. The obtained photoresponsivity value from the photocurrent was 9 mA/W. Similarly, the external quantum efficiency and detectivity values were 1% and 5.4×10^{10} Jones, respectively.

Frequency-dependent transient photocurrent measurements were conducted to examine the stability and reversibility of the photoresponse behavior of the photodiode. The measurements were carried out using a 940 nm infrared light-emitting diode (IR LED) modulated with different frequencies by a function generator. The Al/n^+-GaN/n-Si/Ag and Al/n-GaN/n-Si/Ag photodiodes were connected to a Tektronix TBS2102B digital storage oscilloscope through a photodiode amplifier (ThorLabs PDA200C). Transient photocurrent measurements were performed over a frequency range from 1 kHz to 100 kHz, and in Figs. 7a, b, 8a, and b, normalized photocurrent graphs of both the Al/n^+-GaN/n-Si/Ag and Al/n-GaN/n-Si/Ag photodiodes obtained from transient photocurrent measurements, respectively. The graph of signal amplitude against modulation frequency is illustrated and presented in Figs. 7c and 8c. The cutoff frequency is an essential parameter for determining the actual operating range of the photodiode. The 3 dB frequency point corresponds to the frequency at which the photocurrent drops to 70.71% of its initial value[67–70]. The Al/n^+-GaN/n-Si/Ag and the Al/n-GaN/n-Si/Ag photodiodes exhibited a −3 dB bandwidth of approximately 14.5 kHz and 7.5 kHz at modulation frequencies, respectively.

The rise and fall times of the photodiode, defined as the time difference for the photocurrent signal to rise from 10% to 90% and vice versa, were provided in Figs. 7d and 8d for the Al/n^+-GaN/n-Si/Ag and the Al/n-GaN/n-Si/Ag [68]. As seen in Fig. 7**d,** the rise and fall times for Al/n^+-GaN/n-Si/Ag were determined to be τ_r = 33.8 µs, τ_f = 33.0 µs. Also, as seen in Fig. 8**d**, rise and fall times were calculated as τ_r = 34.8 µs, τ_f = 78.7 µs for Al/n-GaN/n-Si/Ag. Illumination power-dependent photocurrent measurements were conducted under zero-bias conditions with a setup that consists of a 976 nm fiber laser, ThorLabs MC2000B optical chopper controller, and a MC1F10 optical chopper blade. Illumination intensities were varied by driving the using with five different laser powers. Illumination intensities on the photodiodes were recorded as 4.7, 16.1, 26.7, 38.0, and 43.2 mW/cm2 using a Thorlabs PM100D Compact Power and Energy Meter Console and S401C Thermal Power Sensor Head. Figs. 7e and 8e show transient photocurrent graphs of both photodiode devices at a frequency of 500 Hz as a function of illumination powers. To understand the relationship between optical illumination power (P) and photocurrent (I_{ph}), the curve $I_{ph} \propto P^{\alpha}$ is fitted. Here, α is the coefficient. In Figs. 7f and 8f, the fitted coefficients for the relationship between I_{ph} and P are obtained as α=0.341 and α=0.481, respectively. The non-linear power dependency of the photocurrent reflects the significant impact of trap states that are prevalent in the photoconductive mechanism [68,70–72].

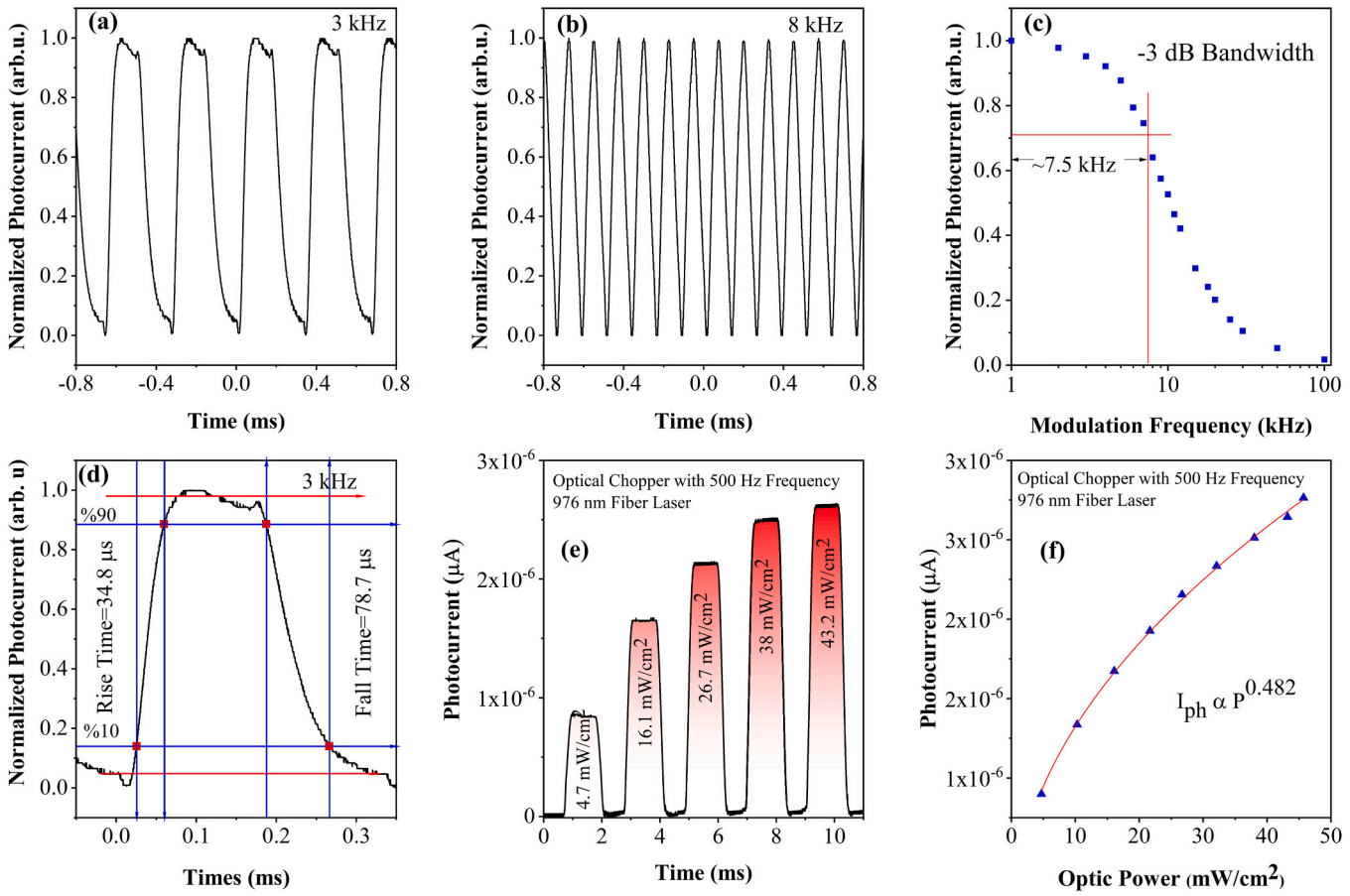


Fig. 8. Transient photocurrent was investigated during the illumination of an Al/n-GaN/n-Si/Ag photodiode, employing a 940 nm infrared light-emitting diode (LED) modulated by a function generator for (a) 3 kHz and (b) ~8 kHz cut off frequency (c) modulation frequency dependence of normalized photocurrent and 3 dB bandwidth of the device at zero bias. (d) Normalized photocurrent in one cycle to show the rise and fall time. (e) Photocurrent with 976 nm fiber laser at different powers at the optical chopper with 500 Hz frequency (f) Photocurrent as a function of the power of incident light for 976 nm fiber laser.

4. Conclusion

In this study, n-type GaN thin films were grown on n-Si wafers using the TE method to produce n^+-GaN/n-Si (as-deposited GaN) n-GaN/n-Si (annealed GaN) isotype PDs. The characteristics of the produced thin films were examined using FESEM, XRD, XPS, Hall Effect, PL, and UV-Vis spectrophotometer. The as-deposited thin films exhibited a transmittance of approximately 5% at a wavelength of 550 nm, and their carrier concentration was determined as 6.17×10^{22} cm^{-3}. The transmittance of the annealed thin films was observed to increase up to 80% at 550 nm wavelength, and the carrier concentration was observed to decrease to 2.3×10^{12} cm^{-3}. XPS analysis also supported the enhancement of the molecular structure through the annealing process.

When analyzing the photodiode characteristics of the produced devices, it was observed that the Al/n^+-GaN/n-Si/Ag PD exhibited better properties. The isotype n^+-GaN/n-Si PD showed superior near-infrared (NIR) light detection capability at 0 V bias. Measurements indicate that at a wavelength of 1050 nm and with an illumination intensity of 10 mW/cm^2, the photoresponsivity value was 355 mA/W, and the FWHM value was 120 nm. Similarly, the external quantum efficiency (EQE), and the detectivity value at the peak wavelength were calculated as 42% and 6.93×10^{11} Jones, and very fast response speed with ~33 µs rise/fall times. respectively. These values reveal that the n^+-GaN/n-Si heterojunction photodiode can be used as a narrow-band detector in the NIR region, and that the TE technique can be used as a rapid and cost-effective alternative method for manufacturing GaN-based semiconductor devices.

CRediT authorship contribution statement

Sertan Kemal Akay: Writing – review & editing, Supervision, Resources, Project administration, Funding acquisition. **Hüseyin Kaan Kaplan**: Writing – review & editing, Validation, Supervision, Methodology, Investigation. **Ali Olkun**: Writing – original draft, Validation, Methodology, Investigation, Formal analysis, Data curation, Conceptualization. **Nursev Erdogan**: Writing – review & editing, Supervision. **Suat Pat**: Writing – review & editing, Resources. **Muhitdin Ahmetoglu**: Supervision, Resources, Conceptualization.

Declaration of Competing Interest

The authors declare that they have no known competing financial interests or personal relationships that could have appeared to influence the work reported in this paper.

Data Availability

Data will be made available on request.

Acknowledgment

This research was supported by Bursa Uludağ University Scientific Research Projects Coordination Unit under project number "FGA-2023–1176" and the Bursa Uludağ University-TUSAŞ Doctoral Program with TÜBİTAK Project No. 118C100. The author would like to thank both Bursa Uludağ University and TUSAŞ Doctoral Program with

TÜBİTAK.

Appendix A. Supporting information

Supplementary data associated with this article can be found in the online version at doi:10.1016/j.sna.2024.115466.

References

[1] L. Hu, X. Ren, J. Liu, A. Tian, L. Jiang, S. Huang, W. Zhou, L. Zhang, H. Yang, High-power hybrid GaN-based green laser diodes with ITO cladding layer, Photonics Res 8 (2020) 279, https://doi.org/10.1364/prj.381262.

[2] L. Li, K. Nomoto, M. Pan, W. Li, A. Hickman, J. Miller, K. Lee, Z. Hu, S.J. Bader, S. M. Lee, J.C.M. Hwang, D. Jena, H.G. Xing, GaN HEMTs on Si with regrown contacts and cutoff/maximum oscillation frequencies of 250/204 GHz, IEEE Electron Device Lett. 41 (2020) 689–692, https://doi.org/10.1109/LED.2020.2984727.

[3] L.Z. Qiu, S.Y. Wei, H.S. Xu, Z.X. Zhang, Z.Y. Guo, X.G. Chen, S.Y. Liu, D. Wu, L. B. Luo, Ultrathin polymer nanofibrils for solar-blind deep ultraviolet light photodetectors application, Nano Lett. 20 (2020) 644–651, https://doi.org/10.1021/acs.nanolett.9b04410.

[4] Y. Li, Z. Xing, Y. Zheng, X. Tang, W. Xie, X. Chen, W. Wang, G. Li, High-efficiency near-UV light-emitting diodes on Si substrates with InGaN/GaN/AlGaN/GaN multiple quantum wells, J. Mater. Chem. C. Mater. 8 (2020) 883–888, https://doi.org/10.1039/c9tc06138j.

[5] M. Lee, M. Yang, K.M. Song, S. Park, InGaN/GaN blue light emitting diodes using freestanding GaN extracted from a Si substrate, ACS Photonics 5 (2018) 1453–1459, https://doi.org/10.1021/acsphotonics.7b01453.

[6] N. Aggarwal, S. Krishna, S.K. Jain, A. Arora, L. Goswami, A. Sharma, S. Husale, A. Gundimeda, G. Gupta, Impact on photon-assisted charge carrier transport by engineering electrodes of GaN based UV photodetectors, J. Alloy. Compd. 785 (2019) 883–890, https://doi.org/10.1016/j.jallcom.2019.01.198.

[7] P. Li, H. Shi, K. Chen, D. Guo, W. Cui, Y. Zhi, S. Wang, Z. Wu, Z. Chen, W. Tang, Construction of GaN/Ga2O3 p-n junction for an extremely high responsivity self-powered UV photodetector, J. Mater. Chem. C. Mater. 5 (2017) 10562–10570, https://doi.org/10.1039/c7tc03746e.

[8] W. Song, J. Chen, Z. Li, X. Fang, Self-Powered MXene/GaN van der waals heterojunction ultraviolet photodiodes with superhigh efficiency and stable current outputs, Adv. Mater. 33 (2021), https://doi.org/10.1002/adma.202101059.

[9] L. Li, Z. Liu, L. Wang, B. zhang, Y. Liu, J.P. Ao, Self-powered GaN ultraviolet photodetectors with p-NiO electrode grown by thermal oxidation, Mater. Sci. Semicond. Process 76 (2018) 61–64, https://doi.org/10.1016/j.mssp.2017.12.019.

[10] L.S. Vikas, K.A. Vanaja, P.P. Subha, M.K. Jayaraj, Fast UV sensing properties of n-ZnO nanorods/p-GaN heterojunction, Sens Actuators A Phys. 242 (2016) 116–122, https://doi.org/10.1016/j.sna.2016.02.038.

[11] X.X. Chen, X.H. Xiao, Z.F. Shi, R. Du, X.J. Li, Self-powered ultraviolet photodetection realized by GaN/Si nanoheterostructure based on silicon nanoporous pillar array, J. Alloy. Compd. 767 (2018) 368–373, https://doi.org/10.1016/j.jallcom.2018.07.066.

[12] K.M.A. Saron, M.R. Hashim, N. Naderi, N.K. Allam, Interface properties determined the performance of thermally grown GaN/Si heterojunction solar cells, Sol. Energy 98 (2013) 485–491, https://doi.org/10.1016/j.solener.2013.09.028.

[13] L. Su, Room temperature growth of CsPbBr3 single crystal for asymmetric MSM structure photodetector, J. Mater. Sci. Technol. 187 (2024) 113–122, https://doi.org/10.1016/j.jmst.2024.01.003.

[14] L. Su, Y. Zhang, J. Xie, An all-inorganic $CsPbBr_3$ /GaN hetero-structure for a near UV to green band photodetector, J. Mater. Chem. C. Mater. 10 (2022) 1349–1356, https://doi.org/10.1039/D1TC04991G.

[15] T. Yamada, J. Ito, R. Asahara, K. Watanabe, M. Nozaki, T. Hosoi, T. Shimura, H. Watanabe, Improved interface properties of GaN-based metal-oxide-semiconductor devices with thin Ga-oxide interlayers, Appl. Phys. Lett. 110 (2017), https://doi.org/10.1063/1.4990689.

[16] G. Chatzigiannakis, A. Jaros, R. Leturcq, J. Jungclaus, T. Voss, S. Gardelis, M. Kandyla, Broadband wavelength-selective isotype heterojunction n+-ZnO/n-Si photodetector with variable polarity, J. Alloy. Compd. 903 (2022), https://doi.org/10.1016/j.jallcom.2022.163836.

[17] M. Patel, M. Kumar, J. Kim, Polarity flipping in an isotype heterojunction (p-SnS/p-Si) to enable a broadband wavelength selective energy-efficient photodetector, J. Mater. Chem. C. Mater. 6 (2018) 6899–6904, https://doi.org/10.1039/C8TC02188K.

[18] L. Wang, Z. Li, M. Li, S. Li, Y. Lu, N. Qi, J. Zhang, C. Xie, C. Wu, L.-B. Luo, Self-powered filterless narrow-band p–n heterojunction photodetector for low background limited near-infrared image sensor application, ACS Appl. Mater. Interfaces 12 (2020) 21845–21853, https://doi.org/10.1021/acsami.0c02827.

[19] S. Qiao, Y. Liu, J. Liu, G. Fu, S. Wang, High-responsivity, fast, and self-powered narrowband perovskite heterojunction photodetectors with a tunable response range in the visible and near-infrared region, ACS Appl. Mater. Interfaces 13 (2021) 34625–34636, https://doi.org/10.1021/acsami.1c09642.

[20] A. Armin, R.D. Jansen-Van Vuuren, N. Kopidakis, P.L. Burn, P. Meredith, Narrowband light detection via internal quantum efficiency manipulation of organic photodiodes, Nat. Commun. 6 (2015), https://doi.org/10.1038/ncomms7343.

[21] M. Liu, J. Wang, Z. Zhao, K. Yang, P. Durand, F. Ceugniet, G. Ulrich, L. Niu, Y. Ma, N. Leclerc, X. Ma, L. Shen, F. Zhang, Ultra-narrow-Band NIR photomultiplication organic photodetectors based on charge injection narrowing, J. Phys. Chem. Lett. 12 (2021) 2937–2943, https://doi.org/10.1021/acs.jpclett.1c00330.

[22] X. Qiu, Z. Wang, X. Hou, X. Yu, D. Yang, Visible-blind short-wavelength infrared photodetector with high responsivity based on hyperdoped silicon, Photonics Res 7 (2019) 351, https://doi.org/10.1364/prj.7.000351.

[23] A.G. Bhuiyan, Y. Kamada, M.S. Islam, R. Syamoto, D. Ishimaru, A. Hashimoto, RF-MBE growth and orientation control of GaN on epitaxial graphene, Results Phys. 20 (2021), https://doi.org/10.1016/j.rinp.2020.103714.

[24] A.S. Yusof, Z. Hassan, S.S. Ng, M.A. Ahmad, M.A.A.Z. Md Sahar, S.O.S. Hamady, C. Chevallier, The dependence of indium incorporation on specified temperatures in growing InGaN/GaN heterostructure using MOCVD technique, Mater. Res. Bull. 137 (2021), https://doi.org/10.1016/j.materresbull.2020.111176.

[25] J. Laifi, C. Saidi, N. Chaaben, A. Bchetnia, Y. El Gmili, J.P. Salvestrini, Role of the TMG flow rate on the GaN layer properties grown by MOVPE on (hkl) GaAs substrates, Mater. Sci. Semicond. Process 101 (2019) 253–261, https://doi.org/10.1016/j.mssp.2019.06.006.

[26] R. Zhuo, Y. Wang, D. Wu, Z. Lou, Z. Shi, T. Xu, J. Xu, Y. Tian, X. Li, High-performance self-powered deep ultraviolet photodetector based on MoS2/GaN p-n heterojunction, J. Mater. Chem. C. Mater. 6 (2018) 299–303, https://doi.org/10.1039/c7tc04754a.

[27] Y. Zhu, K. Liu, Q. Ai, Q. Hou, X. Chen, Z. Zhang, X. Xie, B. Li, D. Shen, A high performance self-powered ultraviolet photodetector based on a p-GaN/n-ZnMgO heterojunction, J. Mater. Chem. C. Mater. 8 (2020) 2719–2724, https://doi.org/10.1039/c9tc06416h.

[28] M.J. Hampshire, T.I. Pritchard, R.D. Tomlinson, A Null Detecting Frequency Meter Operating in the near Infra-red Using A Cdse-ge Isotype Heterojunction, n.d.

[29] M. Ahmetoglu, M. Ozer, O. Kadirov, S.R. BoydedayevPhotoelectrical characteristic of isotype N +-GaSb / n o-GaInAsSb / N +-GaAlAsSb type II heterojunctıons, 2008.

[30] H.K. Kaplan, S.K. Akay, M. Ahmetoğlu, A novel self-powered filterless narrow-band near-infrared photodiode of Cu2S/Si p+-p isotype heterojunction device with very low visible light noise, Appl. Surf. Sci. 601 (2022), https://doi.org/10.1016/j.apsusc.2022.154217.

[31] L.L. Smith, R.F. Davis, M.J. Kim, R.W. Carpenter, Y. Huang, Microstructure, electrical properties, and thermal stability of Al ohmic contacts to *n* -GaN, J. Mater. Res 11 (1996) 2257–2262, https://doi.org/10.1557/JMR.1996.0286.

[32] H.H. Gullu, Ö. Bayraklı Sürücü, M. Terlemezoglu, D.E. Yildiz, M. Parlak, Frequency effect on electrical and dielectric characteristics of In/Cu2ZnSnTe4/Si/Ag diode structure, J. Mater. Sci.: Mater. Electron. 30 (2019) 9814–9821, https://doi.org/10.1007/s10854-019-01318-9.

[33] H.K. Kaplan, S.K. Akay, Transparent and conducting p-type (CuS)x:(ZnS)1-x thin films produced by thermal evaporation: An efficient broadband Si heterojunction photodiode, Appl. Surf. Sci. 652 (2024) 159330, https://doi.org/10.1016/j.apsusc.2024.159330.

[34] H.K. Kaplan, A. Olkun, S.K. Akay, S. Pat, Si-based photodiode and material characterization of TiO2 thin film, Opt. Quantum Electron 53 (2021), https://doi.org/10.1007/s11082-021-02884-1.

[35] K. Sardar, A.R. Raju, G.N. Subbanna, Epitaxial GaN films deposited on sapphire substrates prepared by the sol–gel method, Solid State Commun. 125 (2003) 355–358, https://doi.org/10.1016/S0038-1098(02)00810-4.

[36] S. Pat, Ş. Korkmaz, S. Özen, V. Şenay, GaN thin film deposition on glass and PET substrates by thermionic vacuum arc (TVA), Mater. Chem. Phys. 159 (2015) 1–5, https://doi.org/10.1016/j.matchemphys.2015.03.043.

[37] S.K. Nayak, M. Gupta, S.M. Shivaprasad, Structural, optical and electronic properties of a Mg incorporated GaN nanowall network, RSC Adv. 7 (2017) 25998–26005, https://doi.org/10.1039/c7ra02315d.

[38] N. Abdel All, Structural and photoluminescence study of thin GaN and AlN/GaN nanowires, J. Mater. Sci.: Mater. Electron. 34 (2023), https://doi.org/10.1007/s10854-023-10297-x.

[39] J.N. Kuznia, J.W. Yang, Q.C. Chen, S. Krishnankutty, M. Asif Khan, T. George, J. Frietas, Low pressure metalorganic chemical-vapor deposition of cubic GaN over (100) GaAs substrates, Appl. Phys. Lett. 65 (1994) 2407–2409, https://doi.org/10.1063/1.112690.

[40] M.J. Shin, M. Kim, G.S. Lee, H.S. Ahn, S.N. Yi, D.H. Ha, A GaN nanoneedle inorganic/organic heterojunction structure for optoelectronic devices, Mater. Lett. 91 (2013) 191–194, https://doi.org/10.1016/j.matlet.2012.10.002.

[41] W.K. Hong, J.I. Sohn, D.K. Hwang, S.S. Kwon, G. Jo, S. Song, S.M. Kim, H.J. Ko, S. J. Park, M.E. Weiland, T. Lee, Tunable electronic transport characteristics of surface-architecture- controlled ZnO nanowire field effect transistors, Nano Lett. 8 (2008) 950–956, https://doi.org/10.1021/nl0731116.

[42] W. Park, W.K. Hong, G. Jo, G. Wang, M. Choe, J. Maeng, Y.H. Kahng, T. Lee, Tuning of operation mode of ZnO nanowire field effect transistors by solvent-driven surface treatment, Nanotechnology 20 (2009), https://doi.org/10.1088/0957-4484/20/47/475702.

[43] A.B. Djurišić, W.C.H. Choy, V.A.L. Roy, Y.H. Leung, C.Y. Kwong, K.W. Cheah, T.K. G. Rao, W.K. Chan, H.F. Lui, C. Surya, Photoluminescence and electron paramagnetic resonance of ZnO tetrapod structures, Adv. Funct. Mater. 14 (2004) 856–864, https://doi.org/10.1002/adfm.200305082.

[44] C. Ozgit-Akgun, E. Goldenberg, A.K. Okyay, N. Biyikli, Hollow cathode plasma-assisted atomic layer deposition of crystalline AlN, GaN and AlxGa1-xN thin films at low temperatures, J. Mater. Chem. C. Mater. 2 (2014) 2123–2136, https://doi.org/10.1039/c3tc32418d.

[45] G. Moldovan, M.J. Roe, I. Harrison, M. Kappers, C.J. Humphreys, P.D. Brown, Effects of KOH etching on the properties of Ga-polar n-GaN surfaces, Philos. Mag. 86 (2006) 2315–2327, https://doi.org/10.1080/14786430500522628.

[46] A. M. Nahhas, Review of GaN nanowires based sensors, Am. J. Nanomater. 8 (2020) 32–47, https://doi.org/10.12691/ajn-8-1-4.

[47] R. Huang, T. Liu, Y. Zhao, Y. Zhu, Z. Huang, F. Li, J. Liu, L. Zhang, S. Zhang, A. Dingsun, H. Yang, Angular dependent XPS study of surface band bending on Ga-polar n-GaN, Appl. Surf. Sci. 440 (2018) 637–642, https://doi.org/10.1016/j.apsusc.2018.01.196.
[48] Y. Zhao, H. Gao, R. Huang, Z. Huang, F. Li, J. Feng, Q. Sun, A. Dingsun, H. Yang, Precise determination of surface band bending in Ga-polar n-GaN films by angular dependent X-Ray photoemission spectroscopy, Sci. Rep. 9 (2019), https://doi.org/10.1038/s41598-019-53236-9.
[49] M. Kumar, A. Kumar, S.B. Thapa, S. Christiansen, R. Singh, XPS study of triangular GaN nano/micro-needles grown by MOCVD technique, Mater. Sci. Eng. B Solid State Mater. Adv. Technol. 186 (2014) 89–93, https://doi.org/10.1016/j.mseb.2014.03.010.
[50] V. Thakur, S.M. Shivaprasad, Electronic structure of GaN nanowall network analysed by XPS, Appl. Surf. Sci. 327 (2015) 389–393, https://doi.org/10.1016/j.apsusc.2014.11.082.
[51] M. Grodzicki, J.G. Rousset, P. Ciechanowicz, E. Piskorska-Hommel, D. Hommel, XPS studies on the role of arsenic incorporated into GaN, Vacuum 167 (2019) 73–76, https://doi.org/10.1016/j.vacuum.2019.05.043.
[52] D. Li, M. Sumiya, S. Fuke, D. Yang, D. Que, Y. Suzuki, Y. Fukuda, Selective etching of GaN polar surface in potassium hydroxide solution studied by x-ray photoelectron spectroscopy, J. Appl. Phys. 90 (2001) 4219–4223, https://doi.org/10.1063/1.1402966.
[53] R. Sporken, C. Silien, F. Malengreau, K. Grigorov, R. Caudano, F.J. Sánchez, E. Calleja, E. Muñoz, B. Beaumont, XPS study of Au/GaN and Pt/GaN contacts, n.d.
[54] M. Kumar, S.K. Pasha, T.C. Shibin Krishna, A.P. Singh, P. Kumar, B.K. Gupta, G. Gupta, Facile synthesis and photoluminescence spectroscopy of 3D-triangular GaN nano prism islands, Dalton Trans. 43 (2014) 11855–11861, https://doi.org/10.1039/c4dt01191k.
[55] R. Wasielewski, M. Grodzicki, J. Sito, K. Lament, P. Mazur, A. Ciszewski, Ru/GaN (0001) interface properties, : Acta Phys. Pol. A, Pol. Acad. Sci. (2017) 354–356, https://doi.org/10.12693/APhysPolA.132.354.
[56] S.S. Pan, Y.X. Zhang, X.M. Teng, G.H. Li, L. Li, Optical properties of nitrogen-doped SnO2 films: effect of the electronegativity on refractive index and band gap, J. Appl. Phys. 103 (2008), https://doi.org/10.1063/1.2908197.
[57] M. Futsuhara, K. Yoshioka, O. Takai, Optical properties of zinc oxynitride thin films, Thin Solid Films 317 (1998) 322–325, https://doi.org/10.1016/S0040-6090(97)00646-9.
[58] T.S. Ngo, D.D. Le, J.-H. Song, S.-K. Hong, Growth and characterization of gallium oxide films grown with nitrogen by plasma-assisted molecular-beam epitaxy, Thin Solid Films 682 (2019) 93–98, https://doi.org/10.1016/j.tsf.2019.05.029.
[59] D. Song, L. Li, B. Li, Y. Sui, A. Shen, Band gap engineering of N-alloyed Ga2O3 thin films, AIP Adv. 6 (2016), https://doi.org/10.1063/1.4954720.
[60] J.-H. Choi, M.-H. Ham, W. Lee, J.-M. Myoung, Fabrication and characterization of GaN/amorphous Ga2O3 nanocables through thermal oxidation, Solid State Commun. 142 (2007) 437–440, https://doi.org/10.1016/j.ssc.2007.03.034.
[61] S. Wang, X. Zhang, Z.C. Feng, Y. Cui, Surface chemical and local electronic properties of Al_xGa_1-xN epi-layers grown by MOCVD, Opt. Express 22 (2014) 17440, https://doi.org/10.1364/oe.22.017440.
[62] S.M. Sze, Yiming Li, Kwok KPhysics of Semiconductor Devices, 2021.
[63] E.H. Rhoderick, R.H. Williams, Metal-Semiconductor Contacts SECOND EDITION, n.d.
[64] R. Pillai, D. Starikov, J. Gandhi, A. Debnath, R. Li, C. Boney, A. Bensaoula, InGaN/silicon heterojunction based narrow band near-infrared detector, J. Vac. Sci. Technol. B, Nanotechnol. Microelectron. Mater. Process. Meas. Phenom. 33 (2015) 011205, https://doi.org/10.1116/1.4904760.
[65] L. Shen, Y. Zhang, Y. Bai, X. Zheng, Q. Wang, J. Huang, A filterless, visible-blind, narrow-band, and near-infrared photodetector with a gain, Nanoscale 8 (2016) 12990–12997, https://doi.org/10.1039/c6nr02902g.
[66] Q. Dai, K. Xu, Y. Peng, W. Lv, Z. Zhao, L. Sun, Y. Wang, Q. Li, H. Zhu, Z. Zhou, C. Gu, Towards high performance visible-blind narrowband near-infrared photodetectors with integrated perovskite light filter, Infrared Phys. Technol. 108 (2020), https://doi.org/10.1016/j.infrared.2020.103358.
[67] J.M. Choi, H.Y. Jang, A.R. Kim, J.D. Kwon, B. Cho, M.H. Park, Y. Kim, Ultra-flexible and rollable 2D-MoS2/Si heterojunction-based near-infrared photodetector: via direct synthesis, Nanoscale 13 (2021) 672–680, https://doi.org/10.1039/d0nr07091b.
[68] L. Zeng, S. Lin, Z. Lou, H. Yuan, H. Long, Y. Li, W. Lu, S.P. Lau, D. Wu, Y.H. Tsang, Ultrafast and sensitive photodetector based on a PtSe2/silicon nanowire array heterojunction with a multiband spectral response from 200 to 1550 nm, NPG Asia Mater. 10 (2018) 352–362, https://doi.org/10.1038/s41427-018-0035-4.
[69] J. Kim, S. Yoon, K.M. Sim, D.S. Chung, Rational design of a junction structure to realize an NIR-selective narrowband organic thin-film photodiode, J. Mater. Chem. C. Mater. 7 (2019) 4770–4777, https://doi.org/10.1039/c9tc00722a.
[70] S. Yang, S. Jiao, Y. Nie, T. Jiang, H. Lu, S. Liu, Y. Zhao, S. Gao, D. Wang, J. Wang, Y. Li, Facile synthesis of bismuth nanoparticles for efficient self-powered broadband photodetector application, J. Mater. Sci. Technol. 126 (2022) 161–168, https://doi.org/10.1016/j.jmst.2022.03.019.
[71] S. Qiao, R. Cong, J. Liu, B. Liang, G. Fu, W. Yu, K. Ren, S. Wang, C. Pan, A vertically layered MoS2/Si heterojunction for an ultrahigh and ultrafast photoresponse photodetector, J. Mater. Chem. C. Mater. 6 (2018) 3233–3239, https://doi.org/10.1039/c7tc05896a.
[72] B. Rahmati, I. Hajzadeh, R. Karimzadeh, S.M. Mohseni, Facile, scalable and transfer free vertical-MoS 2 nanostructures grown on Au/SiO 2 patterned electrode for photodetector application, Appl. Surf. Sci. 455 (2018) 876–882, https://doi.org/10.1016/j.apsusc.2018.06.052.

A. Olkun received his Master's degree from Eskişehir Osmangazi University in 2018. He is currently pursuing his doctoral studies in the Physics Department at Bursa Uludağ University. His research interests encompass semiconductor physics, photonics, and optoelectronics. His current doctoral research focuses on the development and application of optical and electronic devices, aiming to contribute to the advancement of technology and scientific understanding.

H. K. Kaplan received his PhD degree in Physics from Bursa Uludağ University. With expertise in semiconductors and semiconductor devices, Kaplan has dedicated his career to advancing knowledge in semiconductors. He has published numerous articles in reputable journals and has presented at international conferences on Physics and Materials Sciences. His research primarily revolves around optoelectronic and photonic semiconductor devices and materials, with a special emphasis on photodiodes. He finds great joy in working in this field. Currently, Dr. Kaplan serves as a Post-Doc researcher at Uludağ University, Bursa, where he is engaged in the synthesis of semiconductors, graphene, and 2D chalcogenide systems, along with their optoelectronic applications.

S. K. Akay obtained his PhD degree in Physics from Bursa Uludağ University. He currently serves as a full professor in the Physics Department, where he is actively engaged in both research and teaching. S. K. Akay research primarily focuses on fabricating and characterizing the electrical, magnetic, and optical properties of a new class of microelectronic and nanoelectronic devices. His work in this area contributes to advancements in both fundamental understanding and practical applications in the field of semiconductor physics and device engineering.

M. Ahmetoglu received the M.Sc. and Ph.D. degrees in semiconductor physics with the Ioffe, Physical-Technical Institute of the Russian Academy of Sciences, St. Petersburg, Russia in 1987 and 1991, respectively. He was with the Faculty of Physics, Namangan State University, Uzbekistan as lecturer, assistant professor and associated professor until 1997. He joined Bursa Uludag University, Türkiye in 1997. He has been with the Department of Physics, Bursa Uludag University since 2012 as professor. He has authored and co-authored over 30 high-impact papers. He is active in the fields of III-V compound semiconductors, optoelectronics, solid state and fiber lasers, IR photodiodes. He is the head of the Laboratory of Optoelectronics and Semiconductor Physics.

S. Pat received Ph.D. degrees in Physics in the field of Plasma and applications from the University of Eskisehir Osmangazi University. He is the Lecturer and Researcher at Research Laboratories of Plasma Physics and Technologies in Eskisehir Osmangazi University, Physics Department in Turkey. His research interests are focused on: Plasma physics and applications, thin films, thin film characterization. He is the Vice Director of the Research Laboratories of Plasma Physics and Technologies in Eskisehir Osmangazi University.

N. Erdoğan received the Ph.D. degree in Metallurgical Engineering from Middle East Technical University, Ankara, Turkey, in 2017. Nursev's research interests encompass composites, functional coatings, aerospace materials and processing technologies, optoelectronic materials, IR reflective materials, frequency selective surfaces, nano-material based engineering, and microwave absorber materials.